Engineering Journal

Second Quarter 2025 | Volume 62, No. 2

Smarter. Stronger. Steel.

Engineering Journal

American Institute of Steel Construction

Dedicated to the development and improvement of steel construction, through the interchange of ideas, experiences, and data.

Editorial Staff

Editor	Margaret A. Matthew, PE
Managing Editor	Keith A. Grubb, SE, PE
Research Editor	Judy Liu, PhD
Production Editor	Kristin Hall

Officers

Chair
Hugh J. McCaffrey

Vice Chair
Glenn R. Tabolt

Secretary/Legal Counsel
Edward Seglias

President
Charles J. Carter, SE, PE, PhD

Senior Vice Presidents
Scott L. Melnick
Mark W. Trimble, PE

Vice Presidents
Todd Alwood
Brandon Chavel, PE, PhD
Carly Hurd, CAE
Christopher H. Raebel, SE, PE, PhD
Brian Raff

The articles contained herein are not intended to represent official attitudes, recommendations or policies of the Institute. The Institute is not responsible for any statements made or opinions expressed by contributors to this Journal.

The opinions of the authors herein do not represent an official position of the Institute, and in every case the officially adopted publications of the Institute will control and supersede any suggestions or modifications contained in any articles herein.

The information presented herein is based on recognized engineering principles and is for general information only. While it is believed to be accurate, this information should not be applied to any specific application without competent professional examination and verification by a licensed professional engineer. Anyone making use of this information assumes all liability arising from such use.

Manuscripts are welcomed, but publication cannot be guaranteed. All manuscripts should be submitted in duplicate. Authors do not receive a remuneration. Guidelines for authors are printed on the inside back cover.

Engineering Journal (ISSN 0013-8029) is published quarterly. Published by the American Institute of Steel Construction at 130 E Randolph Street, Suite 2000, Chicago, IL 60601.

Copyright 2025 by the American Institute of Steel Construction. All rights reserved. No part of this publication may be reproduced without written permission. The AISC logo is a registered trademark of AISC.

Archives: Search at **aisc.org/ej**. Article downloads are free for current members and are available for a nominal fee for non-members.

TECHNICAL NOTE

A Derivation of the Uniform Force Method for Analysis and Design of Gusset Plate Connections for Vertical Diagonal Bracing

THOMAS S. DRANGER and WILLIAM A. THORNTON

INTRODUCTION

The Uniform Force Method (UFM) for vertical diagonal bracing with gusset plate connections is a statically determinate analysis and design in which there are no moments at the interfaces between column, beam, and gusset, producing economical results. The UFM is characterized by the configuration shown in AISC *Steel Construction Manual* (AISC, 2023) Figure 13-2 and the following six equations from the AISC *Manual*.

$$\alpha - \beta \tan\theta = e_b \tan\theta - e_c \tag{13-1}$$

$$V_{rc} = \frac{\beta}{r} P_r \tag{13-2}$$

$$H_{rc} = \frac{e_c}{r} P_r \tag{13-3}$$

$$V_{rb} = \frac{e_b}{r} P_r \tag{13-4}$$

$$H_{rb} = \frac{\alpha}{r} P_r \tag{13-5}$$

where

$$r = \sqrt{(\alpha + e_c)^2 + (\beta + e_b)^2} \tag{13-6}$$

The necessary geometric constraints and interface shear and normal forces shown in Figures 1, 2, 3, and 4, herein, were defined by second author Thornton. In 1984, he originated the constraint equation, AISC *Manual* Equation 13-1, and the force equations, AISC *Manual* Equations 13-2 through 13-6. These six equations, with a derivation of Equation 13-1, but no derivation of the force equations, were first presented at the AISC National Steel Construction Conference (Thornton, 1991). They subsequently appear in Thornton's T. R. Higgins award-winning lecture paper (Thornton, 1995) and in every AISC *Manual* since the Second Edition LRFD *Manual* (AISC, 1995). A necessarily longer derivation of force equations for a less constrained generalized case with only one gusset control point, rather than two, is given in Appendix A of AISC Design Guide 29, *Vertical Bracing Connections* (Muir and Thornton, 2014).

By introducing the UFM constraint equation, the less constrained case in Design Guide 29 might be reduced to generate the UFM force equations, but that indirect proof has not been published, nor any proof until now. Herein, a short, simple, and direct derivation of the UFM force equations is presented.

GEOMETRIC CONSTRAINT

Figures 1, 2, 3, and 4 are elaborations of AISC *Manual* Figure 13-2. The connection geometry is shown in Figure 1. The slope-intercept form is used to write equations for the three lines passing through point GCP and passing through WP, CCP, and BCP. These lines are labeled (1), (2), and (3)

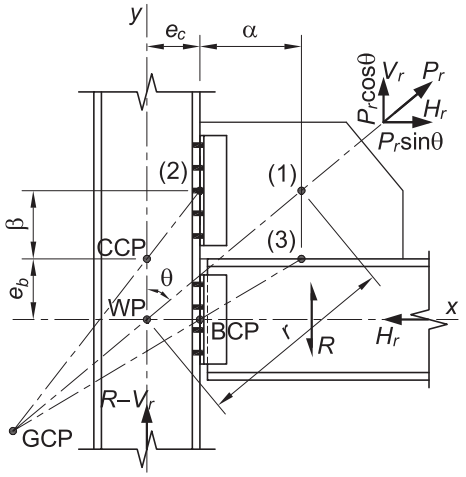

Fig. 1. Connection geometry.

Thomas S. Dranger, PhD, PE, SE, Structural Engineer. Email: dranger@thomasengineers.com (corresponding)

William A. Thornton, PhD, PE, NAE, Retired Corporate Consultant, Cives Engineering, Roswell, Ga. Email: willthorn38@gmail.com

Paper No. 2024-04

in Figure 1 and where they appear in the other figures of this paper. The origin of the coordinate system is at WP, and the equations are written as follows.

Line (1) $$y = \frac{x}{\tan\theta} \tag{1}$$

Line (2) $$y = \frac{\beta}{e_c}x + e_b \tag{2}$$

Line (3) $$y = \frac{e_b}{\alpha}x - \frac{e_b}{\alpha}e_c \tag{3}$$

Eliminate *y* from Equations 1 and 2.

$$\frac{x}{\tan\theta} = \frac{\beta}{e_c}x + e_b \tag{4}$$

$$x = \frac{e_b}{(1/\tan\theta) - (\beta/e_c)} \tag{5}$$

Eliminate *y* from Equations 1 and 3.

$$\frac{x}{\tan\theta} = \frac{e_b}{\alpha}x - \frac{e_b}{\alpha}e_c \tag{6}$$

$$x = \frac{e_b e_c}{e_b - \alpha/\tan\theta} \tag{7}$$

Eliminate *x* from Equations 5 and 7.

$$\frac{e_b e_c}{e_b - \alpha/\tan\theta} = \frac{e_b}{(1/\tan\theta) - (\beta/e_c)} \tag{8}$$

$$\alpha - \beta\tan\theta = e_b\tan\theta - e_c \tag{9}$$

Thus, Equation 13-1 is proven.

INTERNAL FORCES BETWEEN THE GUSSET PLATE, BEAM, AND COLUMN

Once again from the configuration in Figure 1, the distance, *r*, from the origin to the point $(e_c + \alpha, e_b + \beta)$ is expressed by Equation 13-6, rewritten here:

$$r = \sqrt{(\alpha + e_c)^2 + (\beta + e_b)^2} \tag{10}$$

$$\sin\theta = \frac{\alpha + e_c}{r} \tag{11}$$

$$\cos\theta = \frac{\beta + e_b}{r} \tag{12}$$

The horizontal and vertical components of force P_r are:

$$H_r = P_r\sin\theta = \frac{\alpha + e_c}{r}P_r \tag{13}$$

$$V_r = P_r\cos\theta = \frac{\beta + e_b}{r}P_r \tag{14}$$

Referring to the column diagram in Figure 2, sum moments about BCP and use Equation 14 to substitute for V_r.

$$(\beta + e_b)H_{rc} = e_c V_r = \frac{e_c(\beta + e_b)}{r}P_r \tag{15}$$

$$H_{rc} = \frac{e_c}{r}P_r \tag{16}$$

Thus, Equation 13-3 is proven.

Referring to the gusset diagram in Figure 3, sum the horizontal forces and use Equations 13 and 16 to substitute for H_r and H_{rc}.

$$H_{rb} = H_r - H_{rc} = \frac{\alpha + e_c}{r}P_r - \frac{e_c}{r}P_r \tag{17}$$

$$H_{rb} = \frac{\alpha}{r}P_r \tag{18}$$

Thus, Equation 13-5 is proven.

Referring to the beam diagram in Figure 4, sum moments about BCP and use Equation 18 to substitute for Hr_b.

$$\alpha V_{rb} = e_b H_{rb} = \frac{e_b\alpha}{r}P_r \tag{19}$$

$$V_{rb} = \frac{e_b}{r}P_r \tag{20}$$

Thus, Equation 13-4 is proven.

Referring again to the gusset diagram in Figure 3, sum the vertical forces and use Equations 14 and 20 to substitute for V_r and V_{rb}.

$$V_{rc} = V_r - V_{rb} = \frac{\beta + e_b}{r}P_r - \frac{e_b}{r}P_r \tag{21}$$

$$V_{rc} = \frac{\beta}{r}P_r \tag{22}$$

Thus, Equation 13-2 is proven.

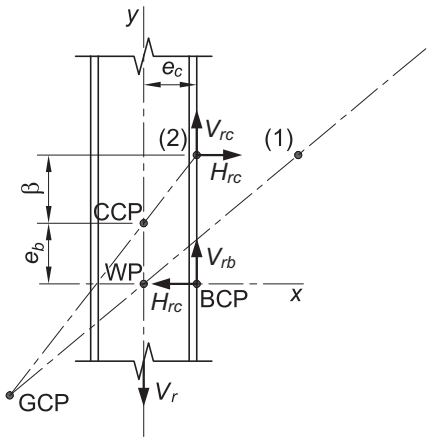

Fig. 2. Column diagram.

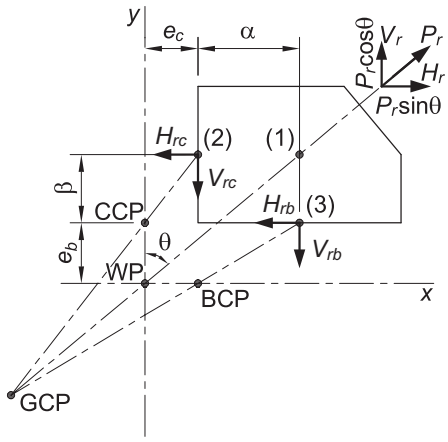

Fig. 3. Gusset diagram.

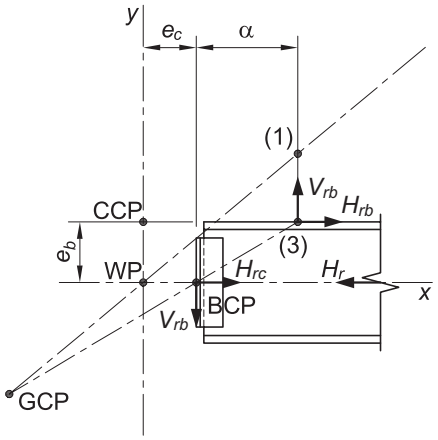

Fig. 4. Beam diagram.

REFERENCES

AISC (1995), *Steel Construction Manual,* 2nd Ed., LRFD, American Institute of Steel Construction, Chicago, Ill, pp. 13-3–13-5.

AISC (2023), *Steel Construction Manual,* 16th Ed., American Institute of Steel Construction, Chicago, Ill, pp. 13-4–13-6.

Muir, L.S. and Thornton, W.A. (2014), *Vertical Bracing Connections*, Design Guide 29, AISC, Chicago, Ill, Chapter 4.

Thornton, W.A. (1991), "On the Analysis and Design of Bracing Connections," *Proceedings of the AISC National Steel Construction Conference*, Washington, D.C., June, pp. 26-1–26-33.

Thornton, W.A. (1995), "Connections: Art and Science, and Information in the Quest for Economy and Safety," *Engineering Journal*, AISC, Vol. 2, No. 4, pp. 132–144.

Block Shear of Bolted Connections—Reliability Analysis and Design Recommendations

BO DOWSWELL

ABSTRACT

In this paper, the existing data from previous research projects was analyzed to determine the reliability of the 2022 AISC *Specification* block shear equations. Additionally, the 1989 AISC *Specification* provisions and the design equations proposed by Driver et al. (2006), Kamtekar (2012), and Teh and Deierlein (2017) were analyzed. The analysis was limited to normal-strength steels. The data set included a total of 279 experimental tests from 25 research projects. For the data set with only U-shaped block shear patterns, the reliability analysis showed that both the 2022 AISC *Specification* and the 1989 AISC *Specification* block shear provisions are conservative.

Based on the results, revisions to the AISC *Specification* were proposed. The proposed design method combines attributes from the available design methods to develop a general design method that is applicable to several common connection types. A secondary intention is to enhance clarity and transparency, where the variables affecting the strength are included explicitly in the equations.

Keywords: block shear, tensile rupture.

INTRODUCTION

Block shear occurs when a connecting element fails around the perimeter of a fastener group as shown in Figure 1. The failure pattern is characterized by tensile rupture at a plane perpendicular to the load and shear failure along either one or two planes parallel to the load.

The analysis by Galambos was used to determine the reliability of the block shear equations that were proposed for the draft of the first AISC LRFD *Specification for Structural Steel Buildings,* hereafter referred to as the AISC *Specification* (1986). After the Galambos report was published, several research projects have significantly expanded the experimental data set for the block shear failure mode. Although the Commentary to 2022 AISC *Specification* Section J4.3 states that the adopted block shear model is conservative, the reliability has not been analyzed using the complete data set.

The objective of this paper is to analyze the existing data from previous research projects to determine the reliability of the 2022 AISC *Specification* block shear equations. Additionally, the 1989 AISC *Specification* provisions and the design equations proposed by Driver et al. (2006), Kamtekar (2012), and Teh and Deierlein (2017) are analyzed. Based on these results, revisions to the AISC *Specification* are proposed.

Bo Dowswell, PE, PhD, Principal, ARC International, LLC, Birmingham, Ala.
Email: bo@arcstructural.com

Paper No. 2024-12

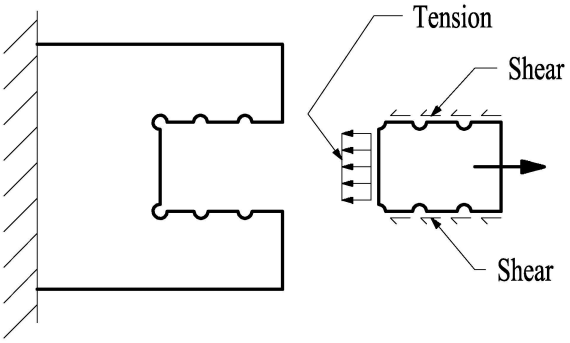

Fig. 1. Block shear.

AISC *SPECIFICATION*

In this section, the 2022 AISC *Specification* equations are presented, and relevant older AISC *Specification* requirements are reviewed. Detailed historical reviews were provided by Epstein and Aleksiewicz (2008) and Geschwinder (2006). Based on the test results of Birkemoe and Gilmor (1978), block shear provisions first appeared in the 1978 AISC *Specification*. Since then, the *Specification* equations changed several times.

The early equations were presented in either ASD or LRFD format with the safety and resistance factors embedded in the equations. However, these equations will be presented in this paper as nominal strengths. Because the safety factors and resistance factors have remained unchanged, using the nominal strength equations results in the most direct comparisons between the various *Specification* requirements. Because the variable symbols have changed, all equations will use the symbols defined in the 2022 AISC *Specification*.

1986 AISC *Specification*

The 1986 AISC *Specification* was the first LRFD specification. The block shear provisions are in Section J4.2.c. Based on the *Specification* verbiage, the block shear strength is the maximum of the two values calculated with Commentary Equations C-J4-1 and C-J4-2. Equations 1a and 1b show the nominal strengths for these equations.

$$R_n = 0.6F_yA_{gv} + F_uA_{nt} \tag{1a}$$

$$R_n = 0.6F_uA_{nv} + F_yA_{gt} \tag{1b}$$

where

A_{gv} = gross area subjected to shear, in.^{2}
A_{gt} = gross area subjected to tension, in.^{2}
A_{nv} = net area subjected to shear, in.^{2}
A_{nt} = net area subjected to tension, in.^{2}
F_u = specified minimum tensile strength, ksi
F_y = specified minimum yield stress, ksi

Galambos (1985) indicated that the draft version of the *Specification* dated 1985 had slightly different block shear equations. His analysis included a nonuniform stress factor, U_{bs}, that was originally proposed by Ricles and Yura (1983). The nonuniform stress factor was applied only to the tension planes as indicated in Equations 2a and 2b. In the draft *Specification*, the block shear strength is the minimum of the two values calculated with Equations 2a and 2b.

$$R_n = 0.6F_yA_{gv} + U_{bs}F_uA_{nt} \tag{2a}$$

$$R_n = 0.6F_uA_{nv} + U_{bs}F_yA_{gt} \tag{2b}$$

Galambos (1985) determined the reliability index for the draft *Specification* to be 3.3 when $\phi = 0.75$ and the live-to-dead-load ratio is $L/D = 3.0$. These results were based on a professional factor that was calculated using the results of 42 experimental tests from four research projects: Birkemoe and Gilmor (1978), Yura et al. (1982), Ricles and Yura (1983), and Hardash and Bjorhovde (1985).

1989 AISC *Specification*

The 1989 AISC *Specification* block shear provisions are in ASD format. Combining Equations J4-1 and J4-2 in Section J4 results in the equation in the Commentary to the 1978 AISC *Specification*. Multiplying by a safety factor of 2.0 results in the nominal block shear strength of Equation 3.

$$R_n = F_uA_{nt} + 0.6F_uA_{nv} \tag{3}$$

2022 AISC *Specification*

In the 2022 AISC *Specification*, the block shear strength is calculated with Equation J4-5, which was first included in the 2005 AISC *Specification*.

$$R_n = 0.6F_uA_{nv} + U_{bs}F_uA_{nt} \le 0.6F_yA_{gv} + U_{bs}F_uA_{nt} \tag{*Spec.* Eq. J4-5}$$

where

U_{bs} = nonuniform stress factor
Ω = 2.00 (ASD)
ϕ = 0.75 (LRFD)

Where the tension stress is uniform, $U_{bs} = 1$; where the tension stress is nonuniform, $U_{bs} = 0.5$. Commentary Figure C-J4.2 indicates that $U_{bs} = 0.5$ for beam shear connections with multiple vertical bolt rows and $U_{bs} = 1$ for all other conditions. The nonuniform stress factor of 0.5 was first recommended by Ricles and Yura (1983), based on the reduced block shear strength and nonlinear stress distribution at the tension plane of bolted clip angle connections with two vertical bolt rows. Although U_{bs} was not included in the 1989 *Specification* block shear provisions, the 50% strength reduction on the tension plane was widely used in practice because it was discussed in *Engineering for Steel Construction* (AISC, 1984) and the *Manual of Steel Construction—Volume II—Connections* (AISC, 1992).

BACKGROUND

This section of the paper provides background information on the *Specification* provisions. It is not intended to provide a complete review of the available research.

Tests by Chesson and Munse (1958, 1963) revealed a limit state with failure around the periphery of fastener (rivets and bolts) groups connecting axially loaded members to gusset plates. Birkemoe and Gilmor (1978) showed experimentally that block shear failure can occur in coped beams with bolted clip angle connections as shown in the L-shaped pattern of Figure 2(a). Marsh (1979) tested 43 bolted double-lap gusset plate connections of steel and aluminum. Marsh was the first to propose a design equation for the U-shaped pattern shown in shown in Figure 2(b). Both the Birkemoe/Gilmor and Marsh research indicated that the block shear strength can be accurately predicted by summing the net rupture strengths of the tension and shear planes.

Tests on 28 bolted gusset plates by Hardash and Bjorhovde (1984, 1985) showed that the limit state is defined by rupture across the tension plane, with various levels of yielding along the shear planes. The extent of shear yielding was dependent on the length of the shear plane. The researchers proposed an empirical equation for the effective shear stress, which varies between the shear yield stress and the shear rupture stresses.

Cunningham et al. (1995) summarized the available test data and concluded that the aspect ratio of the block may have a significant effect on the strength. In cases where the resistance is not symmetrical about the loading plane, the in-plane eccentricity reduces the block shear strength. They noted that the strength can be accurately predicted by summing the net rupture strength of the tension plane and the gross yield strength of the shear planes. Kulak and Grondin (2001) summarized the available test data on gusset plates and came to the same conclusion.

Tests analyzed by Cunningham et al. (1995) and Kulak and Grondin (2001) showed that failure loads of coped beams decrease when the load is applied with an eccentricity relative to the shear failure plane [Figure 3(a)]. This is because the tensile stresses are nonuniform. The triangular stress distribution shown in Figure 3(b) was first recommended by Ricles and Yura (1983) based on their experimental tests.

OTHER DESIGN METHODS

The design methods proposed by Driver et al. (2006), Kamtekar (2012), and Teh and Deierlein (2017) are discussed in this section of the paper.

Driver et al. (2006)

Huns et al. (2002) and Driver et al. (2006) showed that the block shear failure mode consists of shear yielding on the gross section adjacent to the holes, combined with rupture on the net tension area. They proposed Equation 4, where the strength is calculated by combining the net rupture strength of the tension plane with the strength of the shear planes. The shear plane strength is calculated with an effective shear stress, which is the average of the yield and rupture shear stress, applied to the gross shear area.

$$R_n = U_t A_{nt} F_u + 0.6 U_v A_{gv} \left(\frac{F_y + F_u}{2} \right) \tag{4}$$

where

U_t = nonuniform tension stress factor

U_v = nonuniform shear stress factor

For gusset plates with a U-shaped pattern, as shown in Figure 2(b), $U_t = 1$ and $U_v = 1$. When used with a reduction factor of $\phi = 0.75$, This results in a reliability index, β, of 4.4 (Huns et al., 2002). For angles and tees, $U_t = 0.9$ and $U_v = 0.9$. For beam end connections with a single vertical row of bolts, as shown in Figure 2(a), $U_t = 0.9$ and $U_v = 1$. For beam

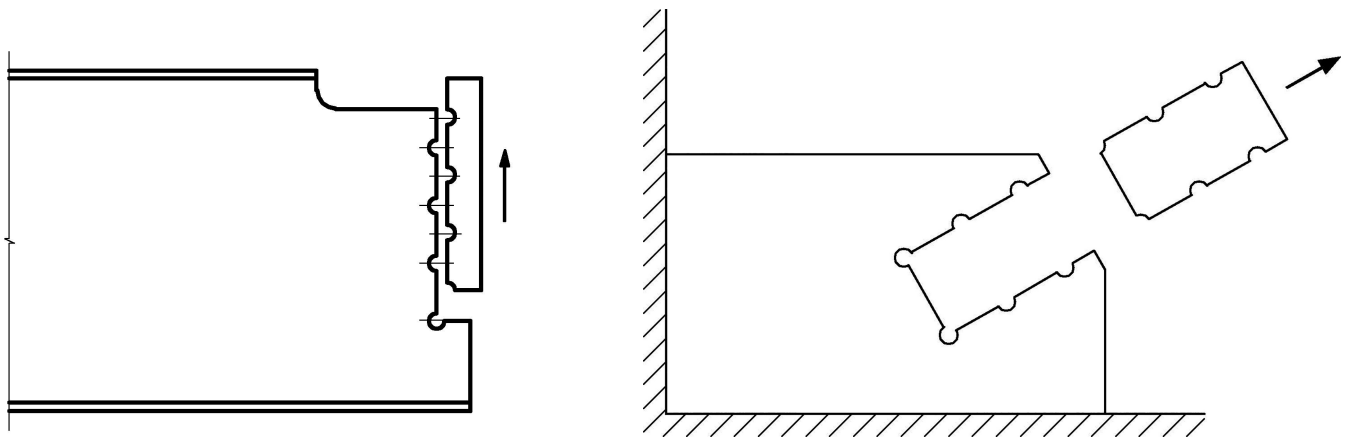

(a) Single-row coped beam *(b) Gusset plate*

Fig. 2. Block shear with uniform tension stress.

Table 1. Nonuniform Tension and Shear Stress Factors		
	U_t	U_v
Gusset plates	1	1
Angles and tee webs	0.9	0.9
Coped beam with one vertical bolt row	0.9	1
Coped beam with two vertical bolt rows	0.3	1

Table 2. Nonuniform Tension Stress Factors, U_t	
Gusset plates	1
Angles and tee webs	0.6
Coped beam with one vertical bolt row	0.9
Coped beam with two vertical bolt rows	0.3

end connections with two vertical rows, as shown in Figure 3(a), $U_t = 0.3$ and $U_v = 1$. The recommended coefficients are summarized in Table 1.

Driver et al. (2006) modified Equation 4 by deleting U_v and recalibrating U_t. This resulted in Equation 5, which is used with the nonuniform tension stress factors in Table 2. Equation 5 was adopted in the Canadian standard, CAN/CSA-S16-14 *Design of Steel Structures* (2014). When used with a resistance factor of $\phi = 0.75$, the resulting reliability index is 4.3 for gusset plates and 3.5 for angles, tee webs, and coped beams. Driver et al. noted that reliability indices less than 4 may be appropriate for the block shear limit state because the ductility is significantly higher than for bolts and welds.

$$R_n = U_t A_{nt} F_u + 0.6 A_{gv}\left(\frac{F_y + F_u}{2}\right) \quad (5)$$

Kamtekar (2012)

The research by Kamtekar (2012) was primarily related to bolt tearout. The tearout strength is calculated using two shear rupture planes between the bolt hole and the member edge. The shear planes are located at the bolt edge, and the shear plane length is calculated using the geometry of the connection (edge distance, bolt diameter, and hole diameter). The same concept was also proposed for the block shear limit state, where the shear area is calculated at the bolt edge as shown in Figure 4.

The block shear strength is calculated with Equation 6.

$$R_n = F_u A_{nt} + 0.6 F_u A_{ev} \quad (6)$$

For connections with round holes, A_{ev} is calculated with a shear length reduction for each hole in the shear plane, l_{vh}, according to Equation 7.

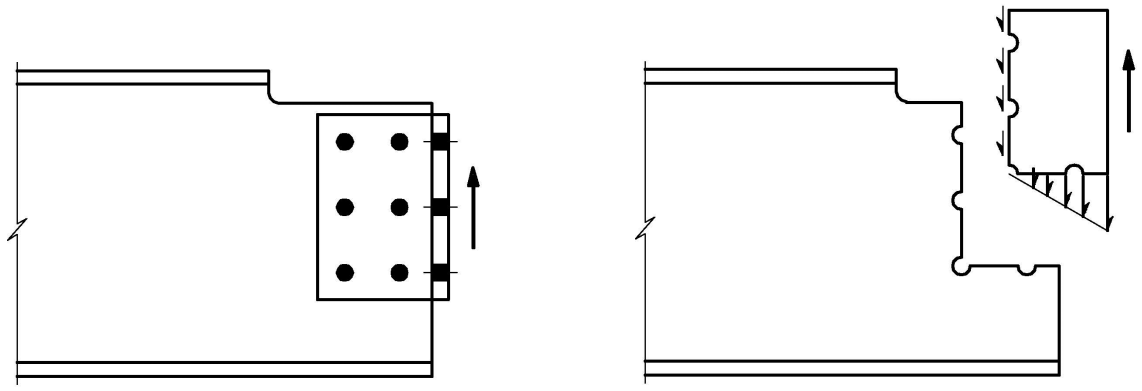

(a) Double-row coped beam *(b) Nonuniform tension stress*

Fig. 3. Block shear of a double-row coped beam web.

$$l_{vh} = \sqrt{d_h^2 - d^2} \quad (7)$$

where

A_{ev} = effective shear area, in.^{2}
d = bolt diameter, in.
d_h = hole diameter, in.

Teh and Deierlein (2017)

The design method proposed by Teh and Deierlein (2017) is based on an effective shear area equal to the average of the gross and net shear areas. The block shear strength is calculated using Equation 6 with the effective shear area calculated with Equation 8.

$$A_{ev} = \frac{A_{gv} + A_{nv}}{2} \quad (8)$$

STATISTICAL PARAMETERS

The objective of this section of the paper is to analyze the existing data from previous research projects. An accurate reliability analysis must consider the actual, measured geometries and material strengths. The bias and variation between actual and specified properties are discussed. The bias coefficient is:

$$\rho_R = \rho_M \rho_G \rho_P \quad (9)$$

where

ρ_G = bias coefficient for the geometric properties, addressing the difference between the nominal and actual dimensions
ρ_M = bias coefficient for the material properties, addressing the difference between the specified and actual strengths
ρ_P = bias coefficient for the test-to-predicted strength ratios; mean value of the professional factor calculated with the measured geometric and material properties

The coefficient of variation is:

$$V_R = \sqrt{V_M^2 + V_G^2 + V_P^2} \quad (10)$$

where

V_G = coefficient of variation for the geometric properties
V_M = coefficient of variation for the material properties
V_P = coefficient of variation for the test-to-predicted strength ratios

Geometric Properties

For the block shear limit state, geometric variations are primarily related to the element thickness. For plate thickness variation, Hess et al. (2002) recommended $\rho_G = 1.05$ with $V_G = 0.044$, and Schmidt and Bartlett (2002) recommended $\rho_G = 1.04$ with $V_G = 0.025$. The values for W-shape webs from Franchuk et al. (2004) are $\rho_G = 1.017$ with $V_G = 0.039$.

Due to a lack of statistical data associated with the effect of fabrication tolerances (hole size, spacing, edge distance) on block shear strength, these variabilities are usually included implicitly in first-order reliability analyses. To consider the effect of geometric variations, including fabrication tolerances, Galambos and Ravinda (1978) recommended $\rho_G = 1.00$ with $V_G = 0.050$. These values, which were used in the block shear reliability analysis by Hardash and Bjorhovde (1984), were also used in this paper.

Material Properties

Recommended statistical parameters for the material tensile strength were summarized by Schmidt and Bartlett (2002). For plates with thicknesses between 10 mm (0.39 in.) and 20 mm (0.79 in.), $\rho_M = 1.19$ with $V_M = 0.034$. These values are conservative compared to those of thicker plates. For I-shaped members, $\rho_M = 1.13$ with $V_M = 0.044$.

Liu et al. (2007) compiled the following tensile strength data:

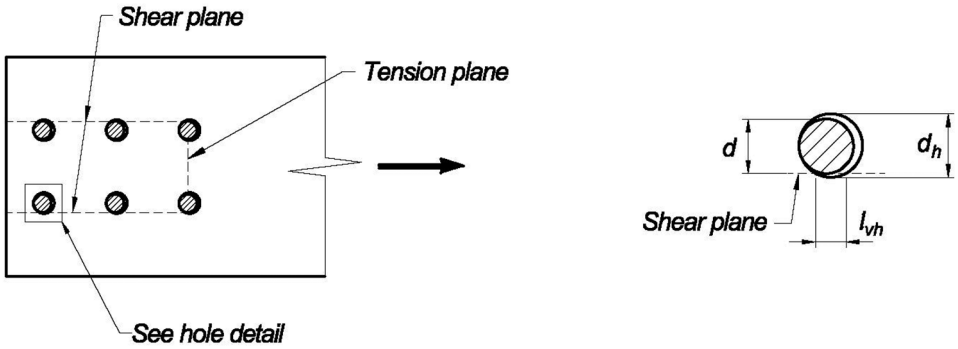

(a) Block shear pattern *(b) Hole detail*

Fig. 4. Kamtekar (2012) block shear pattern.

- For ASTM A992 (2022) W-shapes, $\rho_M = 1.12$ with $V_M = 0.04$. These values are conservative for ASTM A36 (2019a) and ASTM A572 (2021) Grade 50 W-shapes.
- For A572 Grade 50 angles, $\rho_M = 1.38$ with $V_M = 0.06$. The worst case is for A36 angles, where $\rho_M = 1.22$ with $V_M = 0.04$.
- For A36 channels, $\rho_M = 1.18$ with $V_M = 0.04$. However, the preferred material specification in AISC *Manual* (AISC, 2023) Table 2-4 is A992.
- The mean values for ASTM A529 (2019b) and A572 plates are $\rho_M = 1.21$ with $V_M = 0.04$. The worst case is for A572 Grade 55 plates, where $\rho_M = 1.15$ with $V_M = 0.01$.

Recommended statistical parameters for the material yield strength were summarized by Schmidt and Bartlett (2002). For plates with thicknesses between 10 mm (0.39 in.) and 20 mm (0.79 in.), $\rho_M = 1.11$ with $V_M = 0.054$. These values are conservative for thicker plates. For I-shaped members, $\rho_M = 1.03$ with $V_M = 0.063$.

Liu et al. (2007) compiled the following yield strength data:

- For A992 W-shapes, $\rho_M = 1.10$ with $V_M = 0.05$. These values are conservative for A36 and A572 Grade 50 W-shapes.
- For A572 Grade 50 angles, $\rho_M = 1.29$ with $V_M = 0.07$. These values are conservative for A36 and ASTM A588 (2024) angles.
- For A36 channels, $\rho_M = 1.36$ with $V_M = 0.06$. However, the preferred material specification in AISC *Manual* Table 2-4 is A992.
- The mean values for A529 and A572 plates are $\rho_M = 1.15$ with $V_M = 0.06$. The worst case is for A529 Grade 55 plates, where $\rho_M = 1.10$ with $V_M = 0.05$.

Block shear is a valid limit state for each of the available shapes. Although the shear plane strength in 2022 AISC *Specification* Equation J4-5 is limited by the yield strength, the research discussed in this paper indicates that the block shear strength is more accurately predicted with the tensile strength on both the tension and shear planes. Therefore, the lower-bound bias coefficient for tensile strength, $\rho_M = 1.12$, was used in the analysis with $V_M = 0.044$.

Test-to-Predicted Strength

The bias coefficient and coefficient of variation for the test-to-predicted strength ratios, ρ_P and V_P are discussed in this section of the report. These statistical parameters were calculated using existing data from previous research projects. Only specimens with quasi-static loading were included in the data set. The specimens had measured yield stresses between 33.2 and 79.8 ksi. The measured tensile strengths were between 46.8 and 89.3 ksi.

Table 3 provides a summary of the specimens. The data set included a total of 279 experimental tests from 25 research projects. The third column of Table 3 lists the failure pattern that was observed for each specimen.

The test-to-predicted strength parameters are listed in Table 4. Because the various specimen characteristics result in different eccentricities and failure patterns, an evaluation of each connection type is required. Some of the connection types require a nonuniform stress factor; however, these were not included in the Table 4 values. Therefore, only the groups without eccentricity are expected to be accurate. For the other cases, the statistical parameters will be used to determine nonuniform stress factors that result in the lowest V_P values and an appropriate reliability index. Single-row and double-row terminology refers to the number of bolt rows parallel to the loading direction.

RELIABILITY ANALYSIS

In this section of the paper, the statistical parameters are used to determine the reliability of block shear equations from the 2022 AISC *Specification*, the 1989 AISC *Specification*, Driver et al. (2006), Kamtekar (2012), and Teh and Deierlein (2017). The resistance factor required to obtain a specific reliability level is (Galambos and Ravinda, 1978)

$$\phi = C_R \rho_R e^{-\beta \alpha_R V_R} \tag{11}$$

where

C_R = load ratio correction factor
V_R = coefficient of variation
α_R = separation factor
β = reliability index
ρ_R = bias coefficient

Galambos and Ravinda (1973) recommended a separation factor, α_R, of 0.55. For $L/D = 3.0$, Li et al. (2007) developed Equation 12 for calculating the load ratio correction factor.

$$C_R = 1.40 - 0.156\beta + 0.0078\beta^2 \tag{12}$$

The bias coefficient and the coefficient of variation are calculated using the statistical parameters with Equations 9 and 10, respectively. Equations 9 through 12 are accurate only for large sample sizes; however, many of the data sets consist of only a limited number of tests. To consider the effect of small sample sizes, AISI (2016) uses a correction factor applied to V_p, resulting in a coefficient of variation of

$$V_R = \sqrt{V_M^2 + V_G^2 + C_p V_P^2} \tag{13}$$

Table 3. Experimental Tests			
Reference	**Element**	**Failure Pattern**	***n***
Gusset Plates			
Chesson and Munse (1958)	Shaped gusset plate	U	2
Chesson and Munse (1963)	Shaped gusset plate	U	8
Hardash and Bjorhovde (1984)	Rectangular plate	U	28
Udagawa and Yamada (1998)	Rectangular plate	U	49
Huns et al. (2002)	Rectangular plate	U	5
Mullin and Cheng (2004)	Shaped gusset plate	U	5
Brown et al. (2007)	Rectangular plate	U	26
Zeynali et al. (2017)	Rectangular plate	U	22
Braces			
Madugula and Mohan (1988)	Angle brace	L	12
Epstein (1992)	Angle brace	L	2
Sankisa (1993)	Angle brace	L	18
Gross et al. (1995)	Angle brace	L	13
Orbison et al. (1999)	Angle brace	L	3
Orbison et al. (1999)	Web of T-shaped brace	L	9
Aalberg and Larsen (2000)	Web of I-shaped brace	U	4
Bartels (2000)	Web of T-shaped brace	L	3
Castonguay (2009)	Angle brace	L	3
McNeill and Lloyd (2018)	Web of C-shaped brace	U	1
McNeill and Lloyd (2018)	Angle brace	L	1
Pizzuto (2019)	Flange of I-shaped brace	L	7
Jiang et al. (2020)	Angle brace	L	11
Ke et al. (2022)	Angle brace	L	5
Ke et al. (2022)	Angle brace	U	1
Beams			
Birkemoe and Gilmor (1978)	Coped beam	L	1
Yura et al. (1982)	Coped beam	L	4
Ricles and Yura (1983)	Coped beam	L	7
Aalberg and Larsen (2000)	Coped beam	L	8
Franchuk et al. (2004)	Coped beam	L	15
Fang et al. (2013)	Coped beam	L	10
n = sample size			

Table 4. Test-to-Predicted Strength Parameters					
	AISC *Specification* (2022)	**AISC *Specification* (1989)**	**Driver et al. (2006)**	**Kamtekar (2012)**	**Teh and Deierlein (2017)**
All Specimens (n = 279)					
ρ_P	1.16	1.15	1.03	0.952	0.986
V_P	0.113	0.119	0.138	0.115	0.111
Specimens with U-Shaped Failure Pattern (n = 151)					
ρ_P	1.20	1.19	0.995	1.00	1.02
V_P	0.0755	0.0790	0.0801	0.0675	0.0682
Single-Row Brace (n = 72)					
ρ_P	1.07	1.07	0.988	0.888	0.913
V_P	0.128	0.129	0.204	0.128	0.127
Double-Row Brace (n = 8)					
ρ_P	1.02	1.02	1.17	0.918	0.907
V_P	0.0860	0.0919	0.177	0.0872	0.0835
Single-Row Beam (n = 26)					
ρ_P	1.17	1.14	0.965	0.948	0.980
V_P	0.0885	0.102	0.0756	0.0947	0.0945
Double-Row Beam (n = 15)					
ρ_P	0.885	0.829	0.784	0.760	0.769
V_P	0.167	0.216	0.169	0.197	0.203
n = sample size					

The sample size correction factor for $n \geq 4$ is

$$C_P = \left(1+\frac{1}{n}\right)\left(\frac{m}{m-2}\right) = \left(1+\frac{1}{n}\right)\left(\frac{n-1}{n-3}\right) \quad (14)$$

where

m = degrees of freedom
$= n - 1$
n = number of tests

Equation 14 was originally developed by Hall and Pekoz (1988) and revised by Tsai (1992).

Based on the 2022 AISC *Specification* Section B3.1 Commentary, the primary target reliability index used in this report is 4.0. The use of $\beta = 4.0$ for the block shear limit state is discussed further by Franchuk et al. (2004), Teh and Deierlein (2017), and Yam et al. (2011).

Results

The accuracy of the basic equation, without a nonuniform stress factor, is established using only the data set with a U-shaped failure pattern. This data set includes gusset plates, double-row angle braces, I-shaped brace webs, and a channel brace web. The resistance factors calculated with Equation 11 are listed in Table 5. These values were determined with C_p = 1.02, which was calculated using Equation 14 with n = 151.

For connections with a U-shaped failure pattern, ϕ = 0.95 results in an appropriate reliability level for the AISC (2022, 1989) equations. For the Driver et al. (2006), Kamtekar (2012), and Teh and Deierlein (2017) equations, ϕ = 0.80 is appropriate.

ANALYSIS AND DISCUSSION

In this section of the paper, further analysis of the published research is used to establish the effect of oversize holes, shear plane location and the nonuniform stress factor on the block shear strength.

Oversize Holes

Three specimens with oversize holes were tested by Hardash and Bjorhovde (1984). All three specimens had

Table 5. Resistance Factors for U-Shaped Failure Pattern					
	AISC *Specification* (2022)	AISC *Specification* (1989)	Driver et al. (2006)	Kamtekar (2012)	Teh and Deierlein (2017)
ϕ	0.968	0.954	0.796	0.817	0.833

Table 6. Test-to-Predicted Strength Ratios for Specimens with Oversize Holes					
Specimen	AISC *Specification* (2022)	AISC *Specification* (1989)	Driver et al. (2006)	Kamtekar (2012)	Teh and Deierlein (2017)
16	1.21	1.21	0.999	1.08	1.01
20	1.28	1.28	1.08	1.16	1.09
26	1.26	1.26	1.03	1.12	1.05
Mean	1.25	1.25	1.04	1.12	1.05

U-shaped failure patterns. For these specimens, which had ½-in.-diameter bolts with 11⁄16-in.-diameter holes, the test-to-predicted strength ratios are listed in Table 6. The last row shows the mean values, which are higher than the ρ_P values for the specimens with U-shaped failure pattern in Table 4 for all five design equations. The ratios of the mean value from Table 6 to the ρ_P values from Table 4 vary from 1.03 to 1.12, with the Teh and Deierlein equation resulting in the smallest ratio.

Shear Plane Location

Based on the Birkemoe and Gilmor (1978) recommendations, the net tensile and shear areas have traditionally been calculated along the hole centers. However, Kamtekar (2012) and Teh and Deierlein (2017) showed that, for bolted gusset plate connections, the shear failure plane is located between the center and edge of the holes, resulting in increased shear plane areas.

For connections that are symmetrical about the loading axis, bearing of the bolts on the holes induces a secondary constraining force perpendicular to the load (Wen and Mahmoud, 2017), resulting in the shear plane locations shown earlier in Figure 4. Where this constraint is not available, lateral translation of the block causes the shear plane to shift closer to the hole center, as shown in Figure 5. This effect causes a reduction in the shear plane area when compared to constrained elements. The differences in constrained and unconstrained behavior can be clearly identified in many of the post-test photographs in the references of Table 3.

For constrained connections, the Kamtekar (2012) and Teh and Deierlein (2017) equations result in similar reliabilities, with the Kamtekar equation marginally more accurate based on the parameters for U-shaped failure patterns in Table 4. The Kamtekar equation is based on a theoretical failure mechanism and the Teh and Deierlein equation appears to be an empirical estimate. Due to the lack of significant experimental specimens with oversize holes, an accurate reliability assessment of the two equations for this condition is not available. However, the three data points in Table 6 show that both equations are conservative for this limited data set.

To isolate the shear plane in a U-shaped block shear pattern, Orbison et al. (1999) and Aalberg and Larsen (2000) tested I-shaped brace web specimens with the tension plane cut. The test-to-predicted strength parameters for the test by Aalberg and Larsen and five tests by Orbison et al. are listed in Table 7. Based on the ρ_P and V_P values for the five

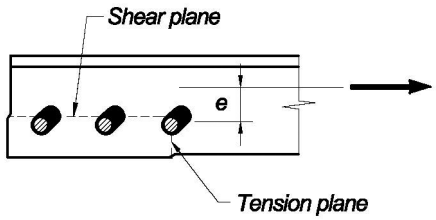

Fig. 5. Nonconstrained connection.

Table 7. Test-to-Predicted Strength Parameters for Shear-Plane Specimens					
	AISC *Specification* (2022)	AISC *Specification* (1989)	Driver et al. (2006)	Kamtekar (2012)	Teh and Deierlein (2017)
Aalberg and Larsen (2000) Test					
Specimen T4-1	1.46	1.46	1.11	1.06	1.14
Orbison et al. (1999) Tests					
Specimen W3	1.27	1.27	1.02	1.00	1.04
Specimen W7	1.31	1.31	1.02	1.01	1.06
Specimen W8	1.25	1.25	0.991	0.978	1.02
Specimen W9	1.25	1.25	1.05	1.02	1.05
Specimen W10	1.17	1.17	0.981	0.952	0.987
Reliability Parameters					
ρ_P	1.29	1.29	1.03	1.00	1.05
V_P	0.0678	0.0678	0.0404	0.0331	0.0471
ϕ	1.01	1.01	0.857	0.843	0.861

block shear equations, the Kamtekar equation is clearly the most accurate.

The tearout limit state for bolted connections occurs when a shear plane rupture occurs parallel to the load on each side of the bolt. The tearout limit state is similar to the block shear limit state without the tension rupture plane. Because there are a significant number of experimental tests available for the tearout limit state, further insight into the behavior of isolated shear planes can be gained by observing these results, which were analyzed by Franceschetti and Denavit (2021). Franceschetti and Denavit indicated that the two effective area methods (Kamtekar, 2012; Teh and Deierlein, 2017) are more accurate than the net area method (AISC, 1989, 2022). They recommended the equation by Kamtekar because it "showed less variation" than the Teh and Deierlein equation and "was found to be accurate over the entire range of hole types investigated."

Nonuniform Stress Factor

Based on the Ricles and Yura (1983) recommendations, the nonuniform stress factor has traditionally been applied to the tension plane resistance. In this study, the accuracy of the nonuniform stress factor was investigated iteratively as a multiplier on the tension term, on the shear term, and to both the tension and shear terms. These comparisons resulted in a minimum coefficient of variation when the nonuniform stress factor was applied to the shear plane resistance. This is because, under some conditions, the block shear strength can be limited by tension plane rupture with a relatively low shear plane efficiency (Cunningham et al. 1995; Orbison et al., 1999; Wen and Mahmoud, 2017).

PROPOSED DESIGN METHOD

Because Equation 3 is simple, transparent, and accurate for many different design conditions, it was used as the basis for the proposed design method. The effective shear area is used in lieu of the net area to allow the use of increased shear areas for laterally constrained elements. A shear plane efficiency factor is used to consider the effect of eccentricity on the shear plane resistance. The nominal strength for the limit state of block shear is

$$R_n = F_u(A_{nt} + 0.6U_vA_{ev}) \tag{15}$$

where

U_v = shear plane efficiency factor

Ω = 1.88 (ASD)

ϕ = 0.80 (LRFD)

Effective Shear Area

For block shear patterns that are symmetrical about the loading axis as shown in Figure 6, the effect of lateral constraint on the shear area can be calculated with an effective hole diameter. For connections with round holes, A_{ev} is calculated with a shear length reduction for each hole in the shear plane, l_{vh}, according to Equation 7. For connections with slotted holes, l_{vh} is the slot dimension parallel to the shear plane. For block shear patterns that are unsymmetrical about the loading axis as shown in Figure 7, A_{ev} should be calculated with the actual hole diameter, d_h. For both symmetrical and unsymmetrical block shear patterns, the net areas should be calculated according to 2022 AISC *Specification* Section B4.3b, which requires "the

Table 8. Reliability Parameters for Eccentric Specimens					
	U_v	n	ρ_P	V_P	ϕ
Single-row brace	1.0	72	1.07	0.129	0.779
Double-row brace	0.90	8	1.06	0.0898	0.818
Single-row beam	1.0	26	1.14	0.102	0.869
Double-row beam	0.30	15	1.26	0.177	0.803
n = sample size					

width of a bolt hole shall be taken as 1⁄16 in. (2 mm) greater than the nominal dimension of the hole."

Eccentricity

The shear plane efficiency factor is used to consider the effect of eccentricity on the shear plane resistance. For the concentrically loaded patterns shown in Figure 6, $U_v = 1.0$. For the eccentrically loaded patterns shown in Figure 7, a reliability analysis is used to calculate the values for U_v to result in $\beta \approx 4$ when $\phi = 0.80$. Table 8 lists the reliability parameters for each connection type. Here, ρ_P and V_P were calculated with Equation 15. The recommended U_v factors are listed in the second column.

CONCLUSIONS

In this paper, the existing data from previous research projects was analyzed to determine the reliability of the 2022 AISC *Specification* block shear equations. Additionally, the 1989 AISC *Specification* provisions and the design equations proposed by Driver et al. (2006), Kamtekar (2012),

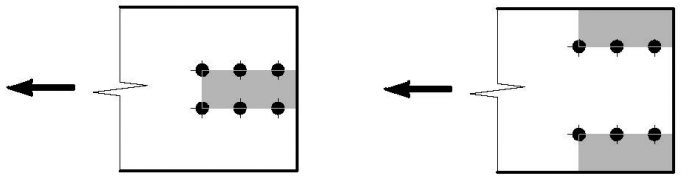

(a) U-shaped pattern *(b) L-shaped pattern*

Fig. 6. Symmetrical block shear patterns.

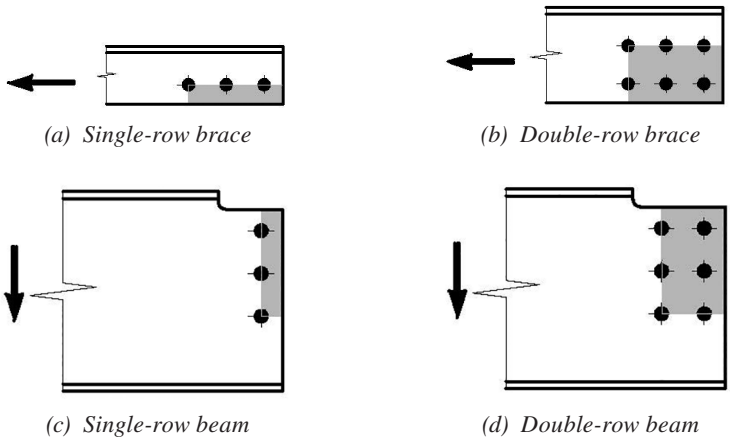

(a) Single-row brace *(b) Double-row brace*

(c) Single-row beam *(d) Double-row beam*

Fig. 7. Unsymmetrical block shear patterns.

and Teh and Deierlein (2017) were analyzed. The analysis was limited to normal strength steels. The data set included a total of 279 experimental tests from 25 research projects. Based on the results, revisions to the AISC *Specification* were proposed.

For the data set with only U-shaped block shear patterns, the reliability analysis showed that both the 2022 AISC *Specification* and the 1989 AISC *Specification* block shear provisions are conservative. Although the 2022 AISC *Specification* requires $\phi = 0.75$, the analysis showed that $\phi = 0.968$ provides an appropriate reliability level. The 1989 AISC *Specification* requires $\Omega = 2.00$; however, $\Omega = 1.50/0.954 = 1.55$ results in adequate reliability. For the Driver et al. (2006), Kamtekar (2012), and Teh and Deierlein (2017) equations, $\phi = 0.80$ is appropriate.

When the data set was expanded to include both U-shaped and L-shaped block shear patterns, the coefficient of variation increased for all five of the design methods that were included in the analysis. This increase is attributed to the effects of lateral constraint and eccentricity, which were considered differently in the various design models.

The proposed design method combines attributes from the available design methods to develop a general design method that is applicable to several common connection types. A secondary intention is to enhance clarity and transparency, where the variables affecting the strength are included explicitly in the equations.

To accurately account for the behavior at failure, F_u is always used to calculate the shear plane strength. This increases the accuracy, simplifies the design equation and eliminates a source of conservatism in the 2022 AISC *Specification* equations.

One source of conservatism in the 2022 AISC *Specification* provisions is the assumption that shear failure occurs along the hole center. That is typically the case for the unsymmetrical (nonconstrained) L-shaped block shear patterns. However, for symmetrical (constrained) U-shaped and L-shaped failure patterns, the shear plane location along the bolt edge increases the shear area. It was concluded that lateral constraint, which is not present at the unsymmetrical L-shaped patterns, is required to cause the shear plane to shift from the hole center to the bolt edge. For nonconstrained connections, the proposed design method is based on the shear area along the hole center. For constrained connections, the shear area along the bolt edge is used. The proposed equations closely model the true location of the shear failure planes for both U- and L-shaped failure patterns.

The block shear strength is also dependent on the loading eccentricity, which is considered with a nonuniform stress factor. In the 2022 AISC *Specification*, the nonuniform stress factor is applied to the tension plane resistance. However, the block shear equations are more accurate when the nonuniform stress factor is applied to the shear plane resistance. A separate reliability analysis was used to calculate these shear plane efficiency factors for four common connection types.

For the proposed design method, the reliability analysis resulted in an appropriate reliability level when $\phi = 0.80$. Compared to the 2022 AISC *Specification* provisions, the proposed design method results in a mean 24% increase in the available strength for connections with U-shaped failure patterns.

REFERENCES

Aalberg, A. and Larsen, P.K. (2000), "Strength and Ductility of Bolted Connections in Normal and High Strength Steels," *Structural Failure and Plasticity*, Proceedings of IMPLAST 2000, Elsevier, pp. 487–494.

AISC (1978), *Specification for the Design, Fabrication and Erection of Structural Steel for Buildings*, American Institute of Steel Construction, Chicago, Ill.

AISC (1984), *Engineering for Steel Construction*, American Institute of Steel Construction, Chicago, Ill.

AISC (1986), *Load and Resistance Factor Design Specification for Structural Steel Buildings*, American Institute of Steel Construction, Chicago, Ill.

AISC (1989), *Specification for Structural Steel Buildings*, American Institute of Steel Construction, Chicago, Ill.

AISC (1992), *Manual of Steel Construction—Volume II—Connections*, American Institute of Steel Construction, Chicago, Ill.

AISC (2005), *Specification for Structural Steel Buildings*, ANSI/AISC 360-05, American Institute of Steel Construction, Chicago, Ill.

AISC (2022), *Specification for Structural Steel Buildings*, ANSI/AISC 360-22, American Institute of Steel Construction, Chicago, Ill.

AISC (2023), *Steel Construction Manual*, 16th Ed., American Institute of Steel Construction, Chicago, Ill.

AISI (2016), *North American Specification for the Design of Cold-Formed Steel Structural Members*, American Iron and Steel Institute, Washington, D.C.

ASTM (2019a), *Standard Specification for Carbon Structural Steel*, ASTM A36/36M, ASTM International, West Conshohocken, Pa.

ASTM (2019b), *Standard Specification for High-Strength Carbon-Manganese Steel of Structural Quality*, ASTM A529/529M, ASTM International, West Conshohocken, Pa.

ASTM (2021), *Standard Specification for High-Strength Low-Alloy Columbium-Vanadium Structural Steel*, ASTM A572/572M-21e1, ASTM International, West Conshohocken, Pa.

ASTM (2022), *Standard Specification for Structural Steel Shapes*, ASTM A992/992M, ASTM International, West Conshohocken, Pa.

ASTM (2024), *Standard Specification for High-Strength Low-Alloy Structural Steel, Up to 50 ksi [345 MPa] Minimum Yield Point, with Atmospheric Corrosion Resistance,* ASTM A588/588M, ASTM International, West Conshohocken, Pa.

Bartels, P.A. (2000), "Net Section Rupture in Tension Members with Connection Eccentricity," Master's Thesis, West Virginia University, Morgantown, Va.

Birkemoe, P.C. and Gilmor, M.I. (1978), "Behavior of Bearing Critical Double-Angle Beam Connections," *Engineering Journal*, AISC, Vol. 15, No. 4, pp. 109–115.

Brown, J.D., Lubitz, D.J., Cekov, Y.C., Frank, K.H., and Keating, P.B. (2007), "Evaluation of Influence of Hole Making Upon the Performance of Structural Steel Plates and Connections," Report No. FHWA/TX-07/0-4624-1, The University of Texas at Austin.

Castonguay, P.X. (2009), "Seismic Performance of Concentrically Braced Steel Frames of the Conventional Construction Category," Master's Thesis, Polytechnique Montréal.

Chesson, E. and Munse, W.H. (1958), "Behavior of Riveted Truss-Type Connections," *Transactions of the American Society of Civil Engineers*, American Society of Civil Engineers, Vol. 123, No. 1.

Chesson, E. and Munse, W.H. (1963), "Riveted and Bolted Joints: Truss-Type Tensile Connections," *Journal of the Structural Division*, American Society of Civil Engineers, Vol. 89, No. ST1.

CSA (2014), *Design of Steel Structures*, Standard S16-14, Canadian Standards Association.

Cunningham, T.J., Orbison, J.G., and Ziemian, R.D. (1995), "Assessment of American Block Shear Load Capacity Predictions," *Journal of Constructional Steel Research*, Vol. 35.

Driver, R.G., Grondin, G.Y., and Kulak, G.L. (2006), "Unified Block Shear Equation for Achieving Consistent Reliability," *Journal of Constructional Steel Research*, Vol. 62.

Epstein, H.I. (1992), "An Experimental Study of Block Shear Failure of Angles in Tension," *Engineering Journal*, AISC, Vol. 29, No. 2, pp. 75–84.

Epstein, H.I. and Aleksiewicz, L.J. (2008), "Block Shear Equations Revisited…Again," *Engineering Journal*, AISC, Vol. 45, No. 1, pp. 5–12.

Fang, C., Lam, A.C.C., Yam, M.C.H., and Seak, K.S. (2013), "Block Shear Strength of Coped Beams with Single-Sided Bolted Connection," *Journal of Constructional Steel Research*, Vol. 86.

Franceschetti, N. and Denavit, M.D. (2021), "Tearout Strength of Concentrically Loaded Bolted Connections," *Engineering Journal*, AISC, Vol. 58, No. 3, pp. 165–184.

Franchuk, C.R., Driver, R.G., and Grondin, G.Y. (2004), "Reliability Analysis of Block Shear Capacity of Coped Steel Beams," *Journal of Structural Engineering*, ASCE, Vol. 130, No. 12, December, pp. 1904–1913.

Galambos, T.V. (1985), "Reliability of Connections, Joints and Fasteners," Structural Engineering Report No. 85-05, Department of Civil and Environmental Engineering, Washington University, St. Louis, Mo.

Galambos, T.V. and Ravinda, M.K. (1973), "Tentative Load and Resistance Factor Design Criteria for Steel Buildings," Research Report No. 18, Department of Civil and Environmental Engineering, Washington University, St. Louis, Mo.

Galambos, T.V. and Ravinda, M.K. (1978), "Load and Resistance Factor Design for Steel," *Journal of the Structural Division*, ASCE, Vol. 104, No. ST9.

Geschwinder, L.F. (2006), "Evolution of Shear Lag and Block Shear Provisions in the AISC Specification," *Engineering Journal*, AISC, Vol. 43, No. 4, pp. 237–240.

Gross, J.M., Orbison, J.G., and Ziemian, R.D. (1995), "Block Shear Tests in High-Strength Steel Angles," *Engineering Journal*, AISC, Vol. 32, No. 3, pp. 117–122.

Hall, B.W. and Pekoz, T. (1988), "Probabilistic Evaluation of Test Results," *Ninth International Specialty Conference on Cold-Formed Steel Structures*, St. Louis, Mo., November 8–9.

Hardash, S.G. and Bjorhovde, R. (1984), *Gusset Plate Design Utilizing Block Shear Concepts*, Department of Civil Engineering and Engineering Mechanics, University of Arizona, Tucson, Az.

Hardash, S.G. and Bjorhovde, R. (1985), "New Design Criteria for Gusset Plates in Tension," *Engineering Journal*, AISC, Vol. 22, No. 2, pp. 77–94.

Hess, P.E. Bruchman, D., Assakkaf, I.A., and Ayyub, B.M. (2002), "Uncertainties in Material Strength, Geometric and Load Variables," *Naval Engineers Journal*, Vol. 114, No. 2.

Huns, B.B.S., Grondin, G.Y., and Driver, R.G. (2002), "Block Shear Behavior of Bolted Gusset Plates," Structural Engineering Report 248, University of Alberta, Canada.

Jiang, D., Yam, M.C.H., Ke, K., Lam, A.C.C., and Zhao, Q. (2020), "Block Shear Failure of S275 and S690 Steel Angles with Single-Line Bolted Connections," *Journal of Constructional Steel Research*, Vol. 170.

Kamtekar, A.G. (2012), "On the Bearing Strength of Bolts in Clearance Holes," *Journal of Constructional Steel Research*, Vol. 79.

Ke, K., Zhang, M., Yam, M.C.H., Lam, A.C.C., Wang, J. and Jiang, B. (2022), "Block Shear Performance of Double-Line Bolted S690 Steel Angles Under Uniaxial Tension," *Thin-Walled Structures*, Vol. 171.

Kulak, G.L. and Grondin, G.Y. (2001), "AISC LRFD Rules for Block Shear in Bolted Connections—A Review," *Engineering Journal*, AISC, Vol. 38, No. 4, pp. 199–203.

Li, C., Grondin, G.Y., and Driver, R.G. (2007), "Reliability Analysis of Concentrically Loaded Fillet Welded Joints," Structural Engineering Report No. 271, University of Alberta, Canada.

Liu, J., Sabelli, R., Brockenbrough, R.L., and Fraser, T.P. (2007), "Expected Yield Stress and Tensile Strength Ratios for Determination of Expected Member Capacity in the 2005 AISC Seismic Provisions," *Engineering Journal*, AISC, Vol. 44, No. 1, pp. 15–25.

Madugula, M.K.S. and Mohan, S. (1988), "Angles in Eccentric Tension," *Journal of Structural Engineering*, ASCE, Vol. 114, No. 10, pp. 2,387–2,396.

Marsh, C. (1979), "Tear-Out Failure of Bolt Groups," *Journal of the Structural Division*, ASCE, Vol. 105, No. ST10.

McNeill, N. and Lloyd, A. (2018), "The Use of Digital Image Correlation to Demonstrate Tension Member Behavior in Structural Steel Design," *CSCE Conference Proceedings*, Canadian Society of Civil Engineers, June 13–16.

Mullin, D.T. and Cheng, J.J.R. (2004), "Ductile Gusset Plates—Tests and Analyses," *Proceedings of the Pacific Structural Steel Conference*, Long Beach, Calif, March 24–27.

Orbison, J.G., Wagner, M.E., and Fritz, W.P. (1999), "Tension Plane Behavior in Single-Row Bolted Connections Subjected to Block Shear," *Journal of Constructional Steel Research*, Vol. 49, pp. 225–239.

Pizzuto, D. (2019), "Block Shear Failures in W-Section Tension Members Connected by Bolted Flange Plates," Master's Thesis, Department of Civil Engineering and Applied Mechanics, McGill University, Montreal, Canada.

Ricles, J.M. and Yura, J.A. (1983), "Strength of Double-Row Bolted-Web Connections," *Journal of Structural Engineering*, ASCE, Vol. 109, No. 1.

Sankisa, K.K. (1993), "Compressive Resistance and Block Shear Strength of Angles," Master's Thesis, Department of Civil and Environmental Engineering, University of Windsor, Ontario, Canada.

Schmidt, B.J. and Bartlett, F.M. (2002), "Review of Resistance Factor for Steel: Data Collection," *Canadian Journal of Civil Engineering*, Vol. 29.

Teh, L.H. and Deierlein, G.G. (2017), "Effective Shear Plane Model for Tearout and Block Shear Failure of Bolted Connections," *Engineering Journal*, AISC, Vol. 54, No. 3, pp. 181–194.

Tsai, M. (1992), "Reliability Models of Load Testing," PhD Dissertation, University of Illinois at Urbana-Champaign, Urbana, Ill.

Udagawa, K., and Yamada, T. (1998), "Failure Modes and Ultimate Tensile Strength of Steel Plates Jointed with High-Strength Bolts," *Journal of Structural and Construction Engineering*, Transactions of AIJ, Architectural Institute of Japan, No. 505.

Wen, H. and Mahmoud, H. (2017), "Simulation of Block Shear Fracture in Bolted Connections," *Journal of Constructional Steel Research*, Vol. 134, pp. 1–16.

Yam, M.C.H., Grondin, G.Y., Wei, F., and Chung, K.F. (2011), "Design for Block Shear of Coped Beams with a Welded End Connection," *Journal of Structural Engineering*, ASCE, Vol. 137, No. 8.

Yura, J.A., Birkemoe, P.C., and Ricles, J.M. (1982), "Beam Web Shear Connections: An Experimental Study," *Journal of Structural Engineering*, ASCE, Vol. 108, No. ST2.

Zeynali, Y., Samimi, M.J., Mazroei, A., Marnani, J.A., and Rohanimanesh, M.S. (2017), "Experimental and Numerical Study of Frictional Effects on Block Shear Fracture of Steel Gusset Plates with Bolted Connections," *Thin-Walled Structures*, Vol. 121.

Steel Structures Research Update

Investigation of Bearing and Tearout of Steel Bolted Connections

JUDY LIU

INTRODUCTION

Recently completed research on bearing and tearout of steel bolted connections is highlighted. This study, conducted at the University of Tennessee, Knoxville, was led by Dr. Mark Denavit, Associate Professor in the Department of Civil and Environmental Engineering. Dr. Denavit's research interests include structural steel connections, stability analysis and design, and innovative seismic systems. Among Dr. Denavit's accolades are the Terry Peshia Early Career Faculty Award (AISC) and the Sarada M. and Raju A. Vinnakota Award (SSRC). AISC supported this research on steel bolted connections. Selected highlights from the completed work are presented.

RESEARCH MOTIVATION AND OBJECTIVES

This research evaluated the behavior and design of steel bolted connections subjected to the limit states of bearing and tearout. The work was motivated by questions about the effective strength approach for bearing-type bolt groups and the accuracy of current tearout strength provisions. A user note introduced in the 2010 AISC *Specification* states that the effective strength of an individual bolt may be taken as the minimum strength computed for bolt shear rupture, bearing, and tearout limit states. The sum of the individual bolt effective strengths is the bolt group strength. Consideration of the interaction of bolt shear rupture, bearing, and tearout is further complicated by tearout strengths that can vary by bolt. Meanwhile, studies on concentrically loaded bolt groups have produced alternative tearout strength equations (Clements and Teh, 2013; Kamtekar, 2012). Dr. Denavit's group sought to improve design of bolted connections by addressing knowledge gaps and developing more accurate methods that capture the influence of tearout.

Judy Liu, PhD, Research Editor of the AISC *Engineering Journal*, Professor, Oregon State University, School of Civil and Construction Engineering, Corvallis, Ore. Email: judy.liu@oregonstate.edu

This study consisted of two phases exploring behavior and design of concentrically and eccentrically loaded connections. Objectives for the first phase included creating a database of experimental tests, evaluating design equations, conducting experimental testing to address knowledge gaps, and developing recommendations for design. In the second phase, the research team conducted tests on concentrically and eccentrically loaded bolt group configurations not previously studied experimentally. The tests further informed recommendations for design of bolted connections subjected to the limit states of bearing and tearout.

PAST RESEARCH AND ALTERNATIVE EQUATIONS

The database of experimental results created by Dr. Denavit's group included 984 test specimens from 31 studies. Categories of connections included concentrically loaded lap splice connections, concentrically loaded butt splice connections, basic eccentrically loaded bolt groups, and single-plate bolted shear connections. Studies reporting bearing and tearout limit states were prioritized, though only 471 of 899 concentrically loaded specimens failed in bearing or tearout. For eccentrically loaded specimens, bearing failures occurred in approximately half of the tests. By design, tearout failures were not observed. Some limitations of the types of connections and configurations found in the literature motivated testing to address knowledge gaps. Additional database details can be found in Denavit et al. (2021).

The team also evaluated alternative tearout lengths. At the end of a plate or component, current provisions use the clear distance, l_c, measured from the edge of the bolt hole to edge of the material. Tearout failure planes, as shown schematically by the dashed lines in Figure 1, are longer than the clear distance. Kamtekar (2012) proposed an estimate of that tearout length, l_{v1}, defined by a line tangent to the bolt and the distance along that line from the edge of the bolt hole to the edge of the material. Clements and Teh (2013) proposed a tearout length, l_{v2}, equal to the average of the clear distance, l_c, and the edge distance, L_e, from the center of the bolt hole to the edge of the material. Evaluations of tearout capacity using these alternative lengths were

compared to a small set of specimens with tearout failures and showed improved predictions (Elliot et al., 2019).

CONCENTRICALLY LOADED BOLT GROUPS

Concentrically loaded bolt group tests were used to expand the database. The published experiments had focused on specimens with standard holes. In those cases, l_{v1} is greater than l_{v2}, but at most by 7% when minimum edge distance requirements are satisfied. This new inventory of tests explored different types of holes, edge distances, and cases where l_{v1} is greater than or less than l_{v2}.

Test Specimens

Single-bolt splices were tested to investigate the behavior of concentrically loaded bolted connections and to evaluate the alternative tearout lengths. The 22 specimens consisted of a single interior test plate between two pull plates (Figure 2), connected with a ¾-in. snug-tight F3125/F3125M (2023) Gr. A490X bolt. The ASTM A572/A572M (2021) Grade 50 test plates were designed to fail in bearing, tearout, or splitting. Splitting started with a tensile fracture at the end of the plate.

The main parameters studied were type of hole and edge distance. Types of holes included standard holes, holes with minimum clearance, oversized holes, holes with ⅛ in. more clearance than oversized holes, and short-slotted holes oriented perpendicular to the load. The nominal edge distances were 1 in., 1.25 in., 1.5 in., and 2 in. The 2 in. edge distance was chosen because it is larger than the 1.91 in. calculated for the transition from bearing to tearout failure for the ¾ in. bolt in a standard hole. The 1 in. edge distance is the minimum for a ¾ in. bolt in a standard hole. The 1 in. edge distance is not permitted for oversized holes, but this case was still included for those holes to be consistent across tests. One specimen (no clearance, 1.25 in. edge distance) was duplicated to investigate repeatability. The standard hole, 1 in. edge distance specimen was also duplicated, with one specimen tested with bolts left untightened and grease applied to the faying surfaces.

The alternate tearout lengths were considered. For the standard hole and minimum/no clearance cases, l_{v1} is greater than l_{v2}. For the oversized and short-slotted holes, l_{v2} is greater than l_{v1}. More information on test parameters can be found in Denavit et al. (2021).

Test Setup

The tests were conducted using a universal testing machine and complementary displacement measurement devices. The test plate assembly was attached to the machine by bolted filler and connection plates (Figure 2). The relative displacement between the pull plates and test plate was measured by two linear variable displacement transducers (LVDTs) mounted to the pull plates and bearing against tabs on the test plate. Optical markers placed on the bolt, test plate, and pull plates for Optotrak deformation measurements (Figure 2) confirmed the LVDT values and also provided elastic deformations in the plates.

For the test, a preload of 500 lb was applied to put the bolt into bearing. The test bolt was finger tightened before an impact wrench was used to obtain a snug-tight condition. All other bolts within the test set-up were finger tightened. The displacement-control test was conducted at a rate of 0.05 in./min to peak load and continued until almost complete loss of load-carrying capacity. The loss of load was typically due to rupture, signaled by one or two loud sounds.

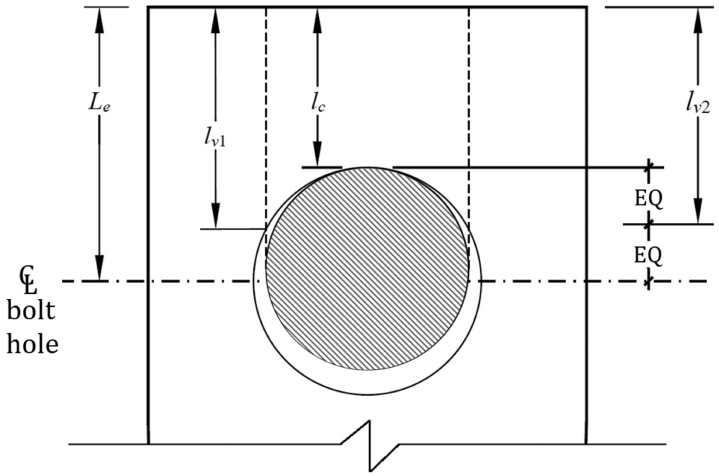

Fig. 1. Tearout lengths.

Results and Discussion

Observed failure mechanisms include splitting tears and shear rupture along one or both sides of the hole (Figure 3). For specimens with short edge distances, the splitting tear continued from the end of the plate to the bolt hole. For test specimens with larger edge distances, the splitting tear did not extend to the bolt hole.

Tested capacities were compared to the predicted values. The strength was evaluated at the ¼ in. deformation limit state and at ultimate. Predicted bolt strengths were calculated using l_{v1} and l_{v2}. The ¼ in. deformation predicted strengths are for the case when deformation at the bolt hole at service load is a design consideration. Test-to-predicted ratios with ¼ in. deformation strengths calculated using l_{v1} and l_{v2} yielded similar results across different hole types. For l_{v1}, the ratios ranged from 0.965 to 1.050, and for l_{v2}, between 0.922 and 1.073. The predicted strengths with l_{v1} and l_{v2} were also more accurate than those using l_c (test-to-predicted ratios from 1.149 to 1.307). At ultimate, the mean test-to-predicted ratios by hole type were more similar between the current equation with l_c and calculations using the alternative tearout lengths. Test-to-predicted values using l_c, for example, ranged from 0.948 to 1.078. However, greater variation was seen for the l_c ratios evaluated across the edge distance values and hole type. Further details and analysis are provided in Franceschetti and Denavit (2021) and Denavit et al. (2021).

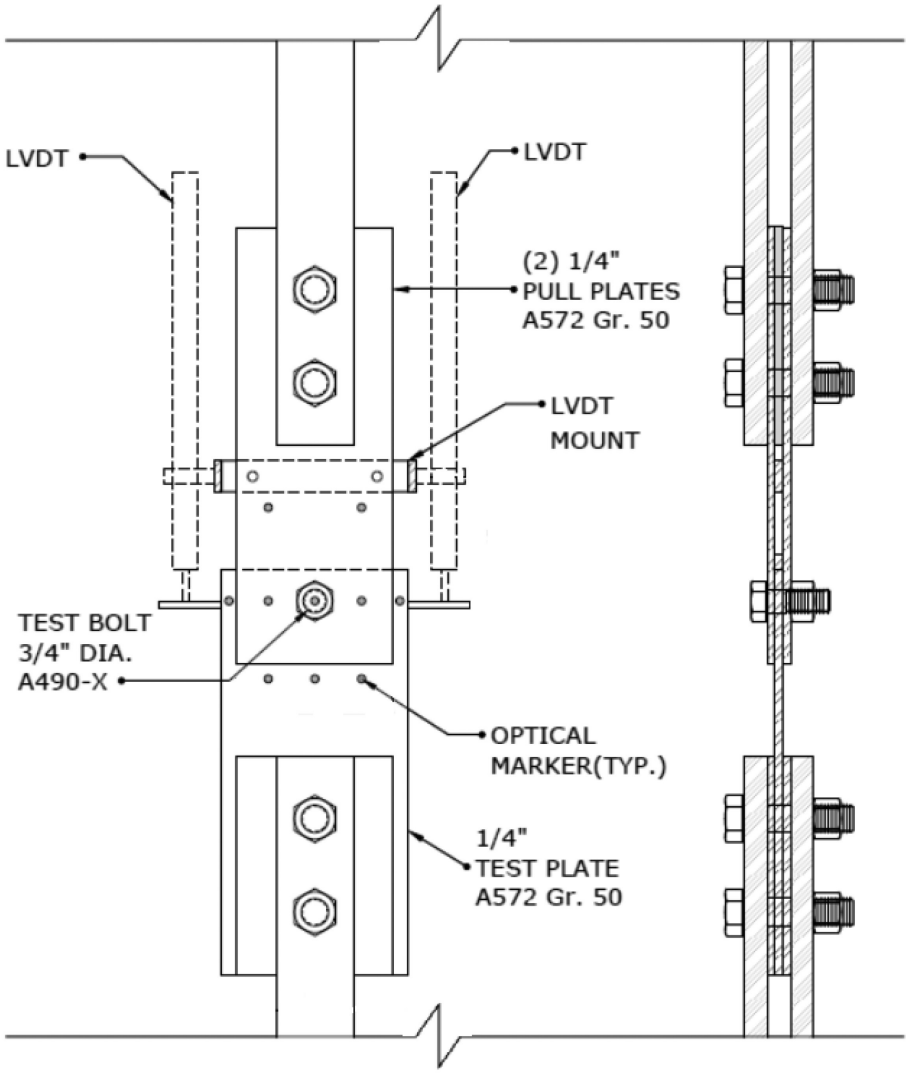

Fig. 2. Elevation and side view of test setup.

Alternative Design Approach

The team also developed an alternative approach for design of concentrically loaded bolted connections. Effective strengths, which can be different for each bolt, are replaced with lower-bound values for edge and interior bolts. The alternative approach leverages the use of t and F_u in both the bearing and tearout equations, recognizing that the bearing-to-tearout strength ratio depends on bolt diameter, d, and clear distance, l_c. This ratio was calculated for the deformation limit state, a range of bolt diameters, and oversize and standard holes. The data was used to develop lower-bound tearout strengths, written in terms of bearing strength, for edge and interior bolts. The approach was adapted to consider bolt shear rupture as well. The derivation of the alternative approach is provided in Denavit et al. (2021).

SINGLE-PLATE SHEAR CONNECTIONS

The single-plate shear connection portion of the study addressed gaps in the literature and questions about current design procedures. Most experimental studies on eccentrically loaded bolt groups, including single-plate connections, did not experience tearout failures because of edge distances or bolt shear rupture. Meanwhile, the approach for design of conventional single-plate shear connections is to neglect the eccentricity and evaluate bearing and tearout as concentric; this approach may be unconservative in some cases. A test program focused on single-plate connections susceptible to tearout failures evaluated the practice of concentric bearing and tearout for the conventional single-plate connections and best methods for predicting the strength of extended single-plate connections.

Modified Instantaneous Center of Rotation Method

The team proposed a modified instantaneous center of rotation method applicable to tearout as well as bolt shear rupture and bearing. The instantaneous center of rotation method accounts for effects of eccentricity within a bolt group, including the resulting magnitude and direction of force at each bolt. The instantaneous center of rotation method had been validated against tests of connections governed by bolt shear rupture and bearing, primarily. The modified method explicitly incorporates the tearout limit state in the ultimate strength calculation of each bolt, using a clear distance calculated based on the direction of force. In cases with sufficient edge distances to preclude tearout, the current and modified methods produce the same results. The team demonstrated how smaller edge distances introducing tearout resulted in a shift of the center of rotation and a reduction in the connection strength. The team also compared their modified instantaneous center of rotation results to the design strengths tabulated for conventional single-plate connections in the AISC *Steel Construction Manual* (2017). They obtained identical results, indicating edge distances large enough to avoid tearout failures and suggesting that the current method for handling tearout for conventional single-plate connections may be appropriate (Denavit et al., 2021). However, experimental investigation is needed to validate the method.

Test Specimens

The single-plate shear connection test matrix was used to further explore the impact of tearout and the viability of different approaches for handling the bearing and tearout limit states. Two conventional and eight extended single-plate connections were tested. The A572 Grade 50

Fig. 3. Concentrically loaded specimen after testing.

plates were ⅜ in. or ½ in. thick. Two-bolt and five-bolt connections used ¾ in. or 1 in. Grade A490-X bolts. The distance, a, from the weld line to the bolt line was set at 3 in. or 9 in. The vertical edge distance, l_{ev}, was set at the minimum value from Table J3.4 in the AISC *Specification for Structural Steel Buildings* (2016). The two conventional connections used a horizontal edge distance, l_{eh}, of two times the bolt diameter. The rest of the connections used the minimum value from Table J3.4.

The test specimens were beam-connection-column subassemblies, with the test connection at one beam end. Beam lengths were 18 ft and 26 ft, and sizes ranged from W8×21 to W18×143. A beam end target rotation of 0.03 rad was set based on the literature. The ASTM A992/A992M (2022) beams were also designed to avoid limit states (e.g., beam yielding) that had been observed in some previous studies. The beam design would ultimately prevent the specimens from reaching the target rotation.

Test Setup

The test specimens were supported and loaded as shown in Figure 4. A frame and hydraulic actuator were located to apply a concentrated load 6 ft from the connection bolt line. Lateral bracing at the beam flanges was provided at intervals not larger than 6 ft. Each test column had single-plate connections welded to each flange (Figure 5) and was used in two test subassemblies. Instrumentation included the load cell and LVDT at the actuator, a load cell at the simple support, two LVDTs, and 12 optical tracking markers at the connection to provide data for calculating rotations. Initial cycles of loading to 2 kips were used to check the instrumentation and data. The specimens were then loaded in displacement control at a rate of 0.1 in./min until failure.

Results and Discussion

Specimen behavior varied and generally did not align with predicted limit states and design strengths. Observed limit states included plate yielding, bolt hole ovalization, bolt shear rupture, tearout, beam yielding, and weld rupture. Test-to-predicted strength ratios, calculated using nominal properties, ranged from 1.71 to 6.11. A root cause for the stronger-than-anticipated connections and some unexpected limit states was the support condition at the column. The rotational restraint at that support shifted the point of zero moment away from the assumed column-face location toward the bolt line, resulting in a lower eccentricity than assumed in design. Additional observations and discussion are provided in Denavit et al. (2021).

DIRECT ECCENTRICALLY LOADED BOLT GROUPS

In the second phase, concentric and eccentric load tests were conducted on configurations not tested previously. The direct eccentrically loaded bolt group tests were designed to address questions not answered by the single-plate shear connection tests and to validate the modified instantaneous center (IC) method. Configurations included concentrically loaded connections with skewed plate edges, plate corners, and connections with only interior bolts placed, as well as different eccentrically loaded bolt groups. Details of the

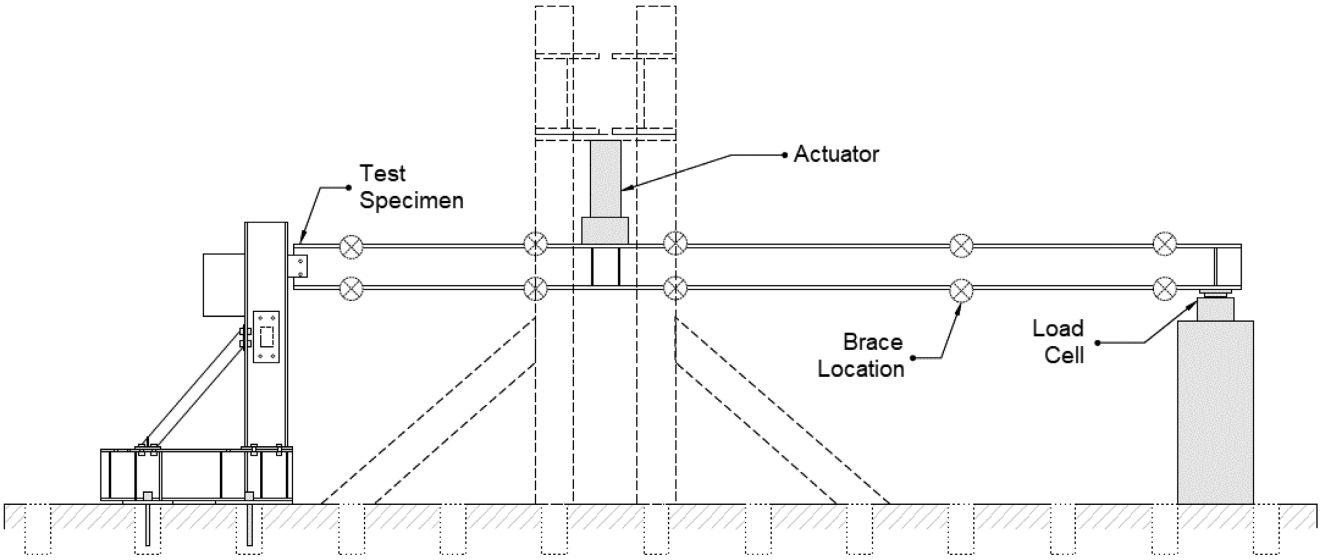

Fig. 4. Test setup for single-plate specimens.

concentrically loaded and eccentrically loaded connection tests are provided in Denavit et al. (2024). Highlights from the eccentrically loaded connection tests are briefly presented.

Test Matrix and Test Setup

This test set focused on relatively large eccentricities for single- and two-row bolted connections. The single-row connection used five ¾ in. A490 bolts. The other connection configuration used the same size and grade of bolts, but in two rows of four. Spacing between bolts and rows was 3 in. Pairs of ¾ in. A572 Gr. 50 plates were connected to the web of an A992 W21×55 (Figure 6). Three edge distances (1.0 in., 1.5 in., and 2.0 in.) were used for each connection configuration for a total of six specimens.

The test setup utilized a wall-mounted actuator and support beam anchored to the strong floor (Figure 6). Three pairs of connector plates transitioned from the welded

Fig. 5. Column and single-plate connection at beam end.

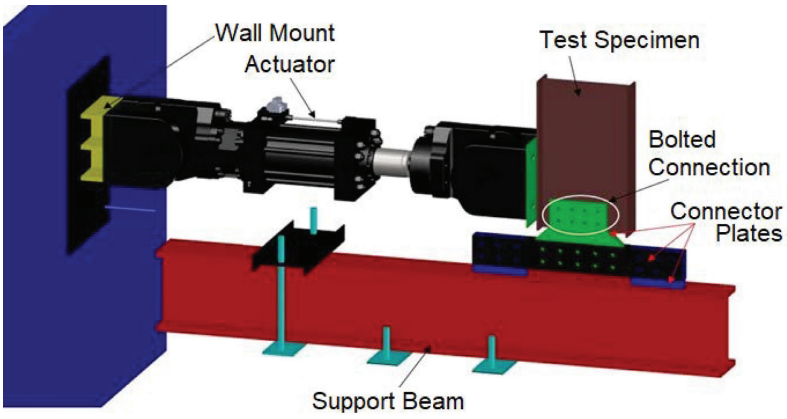

Fig. 6. Test setup for higher eccentricity specimens.

connection at the support beam to the bolted connection at the web of the W21×55 beam. Lateral support was provided by bracing not shown in Figure 6. Displacement-controlled loading was applied at an eccentricity of 9 in. and at a rate of 0.1 in./min. Optical trackers were again used for Optotrak measurements of deformation.

Results and Discussion

The load-deformation responses were similar across the connections. Initial loading saw significant displacement at the low loads as bolts came into bearing, then an increase in stiffness when bolts were in bearing. A linear elastic response followed until yielding in the web resulted in reduced stiffness. The load-deformation plots for one-row bolted connections typically exhibited a sharp drop in load after the peak due to tearout fractures. Two-row specimens maintained their peak load, and the test was stopped before any significant decrease in load. In both connection configurations, the direction of force at each bolt hole is evident, amplified by the bolt hole ovalization, or elongation (Figure 7).

Strength generally increased with edge distance. This increase was more evident for the one-row specimens, as their strength was limited by tearout. In the two-row specimens, the increase in the strength with increased edge distance was more marginal. Yielding and rotation of the web around the two-row bolt group was an indicator of a different ultimate limit state for this connection [Figure 7(b)].

The results were compared to different analysis methods, including the modified instantaneous center of rotation method. The modified IC method correlated well to results for the three one-row specimens with bolt tearout failure. For the IC method not considering tearout, the predictions were unconservative—for example, a 0.614 test-to-predicted ratio at ultimate. The research team determined that the two-row specimens experienced a generalized block shear failure. Equations and discussion of generalized block shear are presented in Jönsson (2014).

EFFECT OF BOLT HOLE CLEARANCE

Research under way is building upon this test program and exploring the impact of bolt hole clearance. Reynolds et al. (2020) extended the IC method to consider hole clearances and the bolt slip and bearing behavior. Their analytical study demonstrated potential strength reductions on the order of 9 to 18% in certain cases. Dr. Denavit's group is conducting experiments to verify the effects of bolt hole clearance predicted by Reynolds et al.

CONCLUSIONS

A comprehensive study evaluated the behavior and design of steel bolted connections subjected to the limit states of bearing and tearout. Through a coordinated experimental and analytical investigation, the research team addressed knowledge gaps and developed methods that capture the influence of tearout. The research demonstrated that neglecting tearout produces unconservative predictions of bolt group capacity. A modified IC method was developed and shown to be more accurate than other methods for bolt groups governed by tearout. For eccentrically loaded two-row bolt groups, generalized block shear failure, a yielding of the material around the bolt group, was identified as the limit state. The bolted connection research continues and includes a study investigating the impact of bolt hole clearance.

ACKNOWLEDGMENTS

Thank you to Dr. Mark Denavit for his many contributions to this article. The work of graduate students Nicolo Franceschetti, Andrew Shahan, Javad Esmaeelpour, and Pratik

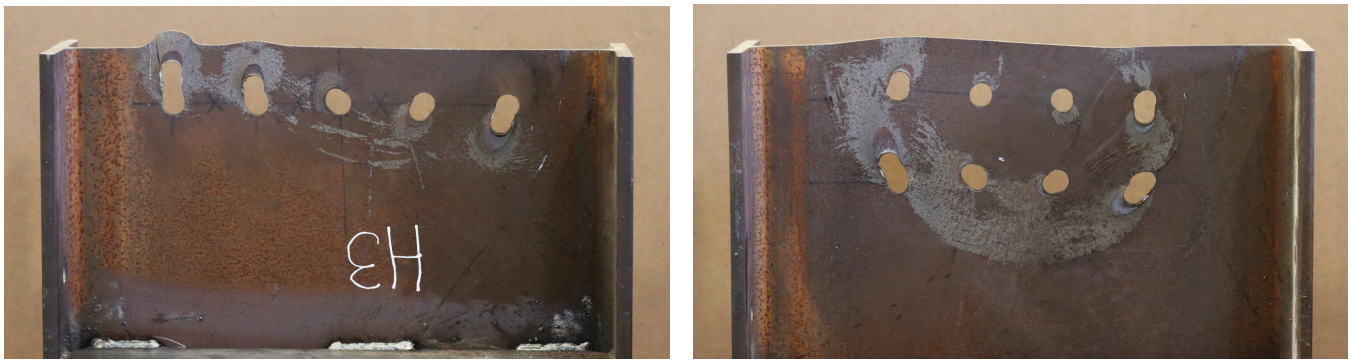

(a) Specimen H3 *(b) Specimen H6*

Fig. 7. Specimens after testing.

Poudel is also acknowledged. The research was funded by the American Institute of Steel Construction (AISC), with in-kind support provided by Cooper Steel and the Siskin Steel & Supply Company. The researchers would also like to thank Alex Moore, Peter Talley, Larry Roberts, and Andy Baker for their assistance with fabrication and testing. Thanks also to Gian Andrea Rassati of the University of Cincinnati, who performed the tests to determine bolt shear strength, and to Devin Huber, Helen McKay, Larry Muir, Bo Dowswell, Patrick McManus, and Brian Volpe for serving on the oversight committee. Any findings or recommendations are those of the researchers and do not necessarily reflect the views of the sponsors.

REFERENCES

AISC (2010), *Specification for Structural Steel Buildings*, ANSI/AISC 360-10, American Institute of Steel Construction, Chicago, Ill.

AISC (2016), *Specification for Structural Steel Buildings*, ANSI/AISC 360-16, American Institute of Steel Construction, Chicago, Ill.

AISC (2017), *Steel Construction Manual,* 15th Ed., American Institute of Steel Construction, Chicago, Ill.

ASTM (2021), *Standard Specification for High-Strength Low-Alloy Columbium-Vanadium Structural Steel*, ASTM A572/572M-21e1, ASTM International, West Conshohocken, Pa.

ASTM (2022), *Standard Specification for Structural Steel Shapes*, ASTM A992/992M, ASTM International, West Conshohocken, Pa.

ASTM (2023), *Standard Specification for High-Strength Structural Bolts and Assemblies, Steel and Alloy Steel, Heat Treated, In. Dimensions 120 ksi and 150 ksi Minimum Tensile Strength, and Metric Dimensions 830 MPa and 1040 MPa Minimum Tensile Strength*, ASTM F3125/3125M, ASTM International, West Conshohocken, Pa.

Clements, D.D.A. and Teh, L.H. (2013), "Active Shear Planes of Bolted Connections Failing in Block Shear," *Journal of Structural Engineering*, Vol. 139, No. 3, pp. 320–327.

Denavit, M.D., Esmaeelpour, J., and Poudel, P. (2024), "Further Investigation of Bearing and Tearout of Steel Bolted Connections," Report to the American Institute of Steel Construction. (Under Review)

Denavit, M.D., Franceschetti, N., and Shahan, A. (2021), "Investigation of Bearing and Tearout of Steel Bolted Connections," Report to the American Institute of Steel Construction.

Elliott, M.D., Teh, L.H., and Ahmed, A. (2019), "Behaviour and Strength of Bolted Connections Failing in Shear," *Journal of Constructional Steel Research*, Vol. 153, pp. 320–329.

Franceschetti, N. and Denavit, M.D. (2021), "Tearout Strength of Concentrically Loaded Bolted Connections," *Engineering Journal,* AISC, Vol. 58, No. 3, pp. 165–183.

Jönsson, J. (2014), "Block Failure in Connections Including Effects of Eccentric Loads," *Proceedings of the 7th European Conference on Steel and Composite Structures* (EUROSTEEL 2014), Naples, Italy.

Kamtekar, A.G. (2012), "On the Bearing Strength of Bolts in Clearance Holes," *Journal of Constructional Steel Research*, Vol. 79, pp. 48–55.

Reynolds, M., Redl, E., and Uang, C.-M. (2020), "Effect of Bolt-Hole Clearance on the Ultimate Strength of Eccentrically Loaded Bolt Groups," *Journal of Structural Engineering*, ASCE. DOI: 10.1061/(ASCE) ST.1943-541X.0002863.

ERRATA

Torsion Design of Round HSS Members—A Critical Review

Bo Dowswell

Vol. 61, No. 3, 2024

In Appendix A, Table A-2, the predicted failure modes for Donnell (1935) Specimens 23 and 24 are incorrect. In the fifth and eighth columns, "I" should be changed to "Y" for these two specimens.

Guide for Authors

Scope

Engineering Journal is dedicated to the improvement and advancement of steel construction. Its pages are open to all who wish to report on new developments or techniques in steel design, research, the design and/or construction of new projects, steel fabrication methods, or new products of significance to the uses of steel in construction. Only original papers should be submitted.

General

Papers intended for publication should be submitted by email Margaret Matthew, editor, at **matthew@aisc.org**.

The articles published in the *Engineering Journal* undergo peer review before publication for (1) originality of contribution; (2) technical value to the steel construction community; (3) proper credit to others working in the same area; (4) prior publication of the material; and (5) justification of the conclusion based on the report.

All papers within the scope outlined above will be reviewed by engineers selected from among AISC, industry, design firms, and universities. The standard review process includes outside review by an average of three reviewers, who are experts in their respective technical area, and volunteers in the program. Papers not accepted will not be returned to the author. Published papers become the property of the American Institute of Steel Construction and are protected by appropriate copyrights. No proofs will be sent to authors.

Manuscripts

Manuscripts must be provided in Microsoft Word format. Include a PDF with your submittal so we may verify fonts, equations and figures. View our complete author guidelines at **aisc.org/ej**.

Smarter. Stronger. Steel.

American Institute of Steel Construction
130 E Randolph St, Ste 2000, Chicago, IL 60601
312.670.2400 | aisc.org/ej